NUMERICAL MODELING OF TWO-DIMENSIONAL HEAT-TRANSFER AND TEMPERATURE-BASED CALIBRATION USING SIMULATED ANNEALING OPTIMIZATION METHOD
Application to Gas Metal Arc Welding

by

Mišo B. BJELIĆ[a]*, Karel KOVANDA[b], Ladislav KOLARIK[b], Miomir N. VUKIĆEVIĆ[a], and Branko S. RADIČEVIĆ[a]

[a] Faculty of Mechanical and Civil Engineering, University of Kragujevac, Kraljevo, Serbia
[b] Faculty of Mechanical Engineering, Czech Technical University, Prague, Czech Republic

Original scientific paper
DOI: 10.2298/TSCI150415127B

Simulation models of welding processes allow us to predict influence of welding parameters on the temperature field during welding and by means of temperature field and the influence to the weld geometry and microstructure. This article presents a numerical, finite-difference based model of heat transfer during welding of thin sheets. Unfortunately, accuracy of the model depends on many parameters, which can not be accurately prescribed. In order to solve this problem, we have used simulated annealing optimization method in combination with presented numerical model. This way, we were able to determine uncertain values of heat source parameters, arc efficiency, emissivity, and enhanced conductivity. The calibration procedure was made using thermocouple measurements of temperatures during welding for P355GH steel. The obtained results were used as input for simulation run. The results of simulation showed that represented calibration procedure could significantly improve reliability of heat transfer model.

Key words: *gas metal arc welding, heat-transfer, temperature, calibration, simulated annealing, optimization*

Introduction

Growing trend of automation of welding processes requires a deep understanding of the influence of welding parameters on heat and mass transfer in the fusion and heat affected zone as well as the influence on the geometry and microstructure of the weld. Modeling of heat transfer during welding is of great importance in order to understand these influences. Two main approaches are analytical and numerical. Most famous of analytical models are those of Rosenthal [1] and Rykalin [2]. But analytical models can not describe heat flow in and near weld pool with proper accuracy [3]. To overcome these difficulties, researchers have started to use numerical heat conduction models [4-7]. Today's models [8-10] describes not only conduction, but also convection, fluid flow, free surface deformation, and arc physics. Group of arc welding processes, which use shielding gases, includes a large number of processes that are applicable for welding of all commercially important materials. One of these processes is gas metal arc welding (GMAW), which is widely used due to its flexibility and

* Corresponding author: bjelic.m@mfkv.kg.ac.rs

productivity. Over the past few decades, GMAW simulation models have developed from relatively simple heat conduction models [11] to very complex models [12-15]. Despite increasing complexity, application of these models is still limited [16, 17]. Main reason is uncertainty of some input parameters like arc efficiency, heat source parameters, and effective conductivity. These uncertainties cause that output of these models is not reliable [16]. Solution to this problem is optimization of input parameters in order to obtain values that will produce outputs, which are in good agreement with experimental results. There are several papers that deals with this problem considering experimental measurements of weld geometry [16-21]. This paper presents a methodology which main goal is to obtain values of input parameters, in this case arc efficiency, heat source parameters and effective conductivity in order to get simulated temperature field as close as possible to experimental values. In order to achieve this goal, we have combine 2-D heat conduction model with global optimization algorithm, in this case simulated annealing. We have used 2-D model in sake of simplicity and computational efficiency. In addition, model deals with temperature-dependent material properties. Simulated annealing as an optimization algorithm allows finding of global optimal values.

Model of heat conduction

Modeling of heat transfer during welding represents a complex problem. Solution to this problem is connected to difficulties related to non-linearities of material physical properties, complexity of boundary conditions, and heat source model. Non-stationary partial differential equation which describes 2-D heat conduction during welding of thin sheets [22] is given by:

$$\frac{\partial T}{\partial \tau} = \frac{\lambda}{c_{\text{eff}}\rho}\left(\frac{\partial^2 T}{\partial x^2} + \frac{\partial^2 T}{\partial y^2}\right) + \frac{1}{c_{\text{eff}}\rho t} q_l - \frac{h_{\text{eq}}}{c_{\text{eff}}\rho t}(T - T_{\text{a}}) \tag{1}$$

Equivalent heat transfer coefficient, h_{eq}, can be calculated according to:

$$h_{\text{eq}} = [h_{\text{u}} + h_{\text{l}} + 2\varepsilon\sigma_c(T + T_{\text{a}})(T^2 + T_{\text{a}}^2)] \tag{2}$$

In case of natural convection, heat transfer coefficient for upper surface of sheets, h_{u}, and heat transfer coefficient for bottom surface of sheets, h_{l}, can be according to [23] calculated:

$$h_{\text{u}} = \frac{\lambda 0.54(\text{Gr Pr})^{1/4}}{l_{\text{k}}}, \qquad h_{\text{l}} = \frac{\lambda 0.27(\text{Gr Pr})^{1/4}}{l_{\text{k}}} \tag{3}$$

where Gr and Pr are Grashof and Prandtl numbers, respectively, and l_{k} is the characteristic length.

Direct application of numerical methods for solution of eq. (1) consequently has a large number of computations in each time step. Therefore, in order to reduce computational efforts, we have used a moving co-ordinate system, fig. 1. Equations (4) and (5) expresses connection between co-ordinate system xyz and co-ordinate system ξyz:

$$\xi = x - v_w\tau, \qquad \frac{\partial \xi}{\partial \tau} = -v_w \tag{4}$$

$$\frac{\partial T(\xi, y, \tau)}{\partial \tau} = \frac{\partial T}{\partial \xi}\frac{\partial \xi}{\partial \tau} + \frac{\partial T}{\partial y}\frac{\partial y}{\partial \tau} + \frac{\partial T}{\partial \tau}\frac{\partial \tau}{\partial \tau} = -v_w\frac{\partial T}{\partial \xi} \tag{5}$$

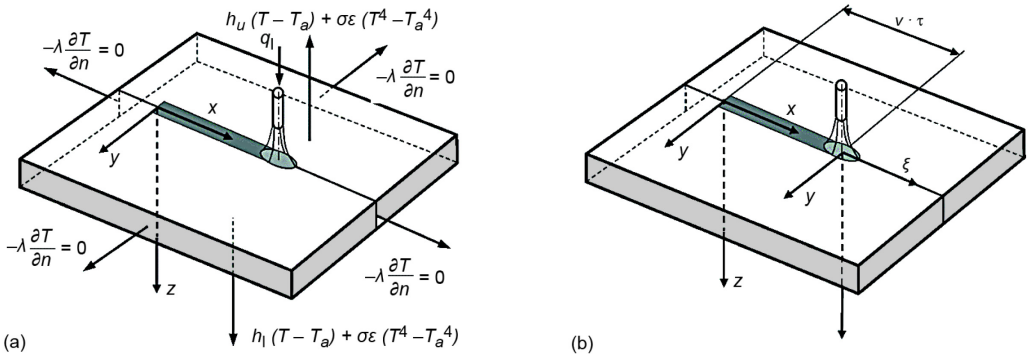

Figure 1. (a) Schematic illustration of GMAW of thin sheets with border conditions, (b) illustration of connection between stationary and moving co-ordinate system

Considering eq. (1) and eqs. (4) and (5), we get quasi-stationary partial differential equation, eq. (6), which describes heat transfer in welded sheets using moving co-ordinate system:

$$-v_w \frac{\partial T}{\partial \xi} = \frac{\lambda}{c_{\text{eff}} \rho} \left(\frac{\partial^2 T}{\partial \xi^2} + \frac{\partial^2 T}{\partial y^2} \right) + \frac{1}{c_{\text{eff}} \rho t} q_l - \frac{h_{\text{eq}}}{c_{\text{eff}} \rho t} (T - T_{\text{a}}) \tag{6}$$

Numerical solution

For numerical solution, we have used a finite difference method. Computational domain is discretized using orthogonal grid. First and second derivative of temperature are replaced by central finite differences:

$$\frac{\partial T}{\partial \xi} = \frac{T_{i+1,j} - T_{i-1,j}}{2\Delta\xi}, \quad \frac{\partial^2 T}{\partial \xi^2} = \frac{T_{i+1,j} - 2T_{i,j} + T_{i-1,j}}{(\Delta\xi)^2}, \quad \frac{\partial^2 T}{\partial y^2} = \frac{T_{i,j+1} - 2T_{i,j} + T_{i,j-1}}{(\Delta y)^2} \tag{7}$$

Replacing eq. (7) into eq. (6), we obtain:

$$T_{i,j} = A(T_{i-1,j} + T_{i+1,j} + T_{i,j-1} + T_{i,j+1}) + B(T_{i+1,j} - T_{i-1,j}) + Cq_l + D \tag{8}$$

For iterative solution of eq. (8), we have used successive over-relaxation method. So, eq. (8) now becomes:

$$T_{i,j}^{k+1} = (1-\omega)T_{i,j}^{k} + \omega[A(T_{i-1,j}^{k+1} + T_{i+1,j}^{k} + T_{i,j-1}^{k+1} + T_{i,j+1}^{k}) + B(T_{i+1,j}^{k} - T_{i-1,j}^{k+1}) + Cq_{l(i,j)} + D] \tag{9}$$

where A, B, C, and D are equal to:

$$A = \frac{\lambda t}{4\lambda t + h_{\text{eq}}\delta^2}, \quad B = \frac{v_w \delta c_{\text{eff}} \rho t}{8\lambda t + 2h_{\text{eq}}\delta^2}, \quad C = \frac{\delta^2}{8\lambda t + 2h_{\text{eq}}\delta^2}, \quad D = \frac{h_{\text{eq}}\delta^2 T_a}{4\lambda t + h_{\text{eq}}\delta^2} \tag{10}$$

Heat source

Interaction between welding arc and molten pool is a complex phenomenon, which is not accurately described, yet. Many authors have developed different heat source models in

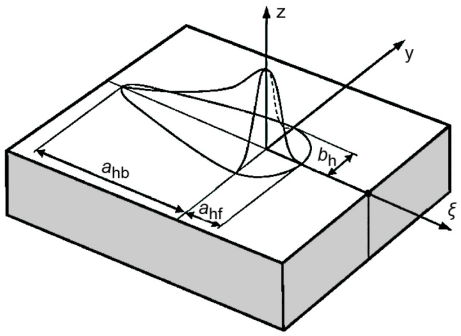

Figure 2. Schematic illustration of double-ellipse surface distribution heat source

order to reduce complexity of arc model to acceptable level. In this case, we have applied double-ellipse surface distribution source [3], fig. 2. The heat density distribution inside front and rear half-ellipse is equal to:

$$q_f(\xi, y, z) = \frac{6 r_f Q}{a_{\mathrm{hf}} b_{\mathrm{h}} \pi} \mathrm{e}^{-3\frac{\xi^2}{a_{\mathrm{hf}}^2}} \mathrm{e}^{-3\frac{y^2}{b_{\mathrm{hf}}^2}} \tag{11}$$

$$q_b(\xi, y, z) = \frac{6 r_b Q}{a_{\mathrm{hb}} b_{\mathrm{h}} \pi} \mathrm{e}^{-3\frac{\xi^2}{a_{\mathrm{hb}}^2}} \mathrm{e}^{-3\frac{y^2}{b_{\mathrm{hf}}^2}} \tag{12}$$

where Q, r_f, and r_b are equal to:

$$Q = \eta U I, \qquad r_f = \frac{a_{\mathrm{hf}}}{a_{\mathrm{hf}} + a_{\mathrm{hb}}}, \qquad r_b = \frac{a_{\mathrm{hb}}}{a_{\mathrm{hf}} + a_{\mathrm{hb}}} \tag{13}$$

Modeling of thermophysical properties

Thermophysical properties needed for solution of eq. (9) are the density, the thermal conductivity, and specific heat. These properties are function of the temperature and the composition of welded plates [24]. Base material, which we used in experiment, was steel P355GH with chemical composition, tab. 1.

Table 1. Chemical composition of base material – P355GH

C	Si	P	S	Mn	Nb
0.20	0.19	0.016	0.062	1.45	0.014

Due to lack of data for given chemical composition, we used Fe-Fe_3C diagram in order to obtain these thermophysical properties. Critical temperatures Ae_1 and Ae_3 are calculated based on [25]:

$$Ae_1 = 723 - 16.9\,\mathrm{Ni} + 29.1\,\mathrm{Si} + 6.38\,\mathrm{W} - 10.7\,\mathrm{Mn} + 16.9\,\mathrm{Cr} + 290\,\mathrm{As} \tag{14}$$

$$\begin{aligned} Ae_3 = {} & 910 - 203\sqrt{C} + 44.7\,\mathrm{Si} - 15.2\,\mathrm{Ni} + 31.5\,\mathrm{Mo} + 104\,\mathrm{V} + 13.1\,\mathrm{W} - \\ & - 30\,\mathrm{Mn} + 11\,\mathrm{Cr} + 20\,\mathrm{Cu} - 700\,\mathrm{P} - 400\,\mathrm{Al} - 120\,\mathrm{As} - 400\,\mathrm{Ti} \end{aligned} \tag{15}$$

Equations for solidus and liquidus temperature are adopted from [26, 27]:

$$\begin{aligned} T_{\mathrm{liq}} = {} & 1536 - (78\,\mathrm{C} + 7.6\,\mathrm{Si} + 4.9\,\mathrm{Mn} + 34\,\mathrm{P} + 30\,\mathrm{S} + 5\,\mathrm{Cu} + \\ & + 3.1\,\mathrm{Ni} + 1.3\,\mathrm{Cr} + 3.6\,\mathrm{Al} + 2\,\mathrm{Mo} + 2\,\mathrm{V} + 18\,\mathrm{Ti}) \end{aligned} \tag{16}$$

$$\begin{aligned} T_{\mathrm{sol}} = {} & 1536 - (415.5\,\mathrm{C} + 12.3\,\mathrm{Si} + 6.8\,\mathrm{Mn} + 124.5\,\mathrm{P} + 183.9\,\mathrm{S} + \\ & + 4.3\,\mathrm{Ni} + 1.4\,\mathrm{Cr} + 4.1\,\mathrm{Al}) \end{aligned} \tag{17}$$

Carbon content, C, of eutectoid alloy can be calculated from condition $Ae_3 = Ae_1$. Carbon content of ferrite is calculated based on Fe-Fe_3C diagram, assuming linear temperature dependencies:

$$\mathrm{C}_\alpha = 0.02\,\frac{T-20}{Ae_1-20},\ \text{for}\ T \le Ae_1 \qquad \text{and} \qquad \mathrm{C}_\alpha = 0.02\,\frac{T-Ae_3(\mathrm{C}=0)}{Ae_1-Ae_3(\mathrm{C}=0)},\ \text{for}\ Ae_1 < T \le Ae_3 \tag{18}$$

Carbon content of austenite is calculated based on eq. (15):

$$\mathrm{C}_\gamma = [(910 + 44.7\,\mathrm{Si} - 15.2\,\mathrm{Ni} + 31.5\,\mathrm{Mo} + 104\,\mathrm{V} + 13.1\,\mathrm{W} - 30\,\mathrm{Mn} + 11\,\mathrm{Cr} + 20\,\mathrm{Cu} - 700\,\mathrm{P} - 400\,\mathrm{Al} - 120\,\mathrm{As} - 400\,\mathrm{Ti}) - T]^2/203^2 \tag{19}$$

While, carbon content of liquid phase can be expressed based on eq. (16):

$$\mathrm{C}_{\mathrm{liq}} = [1536 - (7.6\,\mathrm{Si} + 4.9\,\mathrm{Mn} + 34\,\mathrm{P} + 30\,\mathrm{S} + 5\,\mathrm{Cu} + 3.1\,\mathrm{Ni} + 1.3\,\mathrm{Cr} + 3.6\,\mathrm{Al} + 2\,\mathrm{Mo} + 2\,\mathrm{V} + 18\,\mathrm{Ti}) - T]/78 \tag{20}$$

We have calculated volume fractions of ferrite, pearlite, austenite, and liquid phase using eqs. (18)-(20) and eq. (21), which represents lever rule. Figure 3 shows results of calculations *vs.* temperature.

$$f_\alpha = \frac{\mathrm{C}_{\mathrm{eut}} - \mathrm{C}}{\mathrm{C}_{\mathrm{eut}} - \mathrm{C}_\alpha},\quad f_p = \frac{\mathrm{C} - \mathrm{C}_\alpha}{\mathrm{C}_{\mathrm{eut}} - \mathrm{C}_\alpha},\quad f_\gamma = \frac{\mathrm{C} - \mathrm{C}_\alpha}{\mathrm{C}_\gamma - \mathrm{C}_\alpha},\quad f_{\mathrm{liq}} = \frac{\mathrm{C} - \mathrm{C}_\gamma}{\mathrm{C}_{\mathrm{liq}} - \mathrm{C}_\gamma} \tag{21}$$

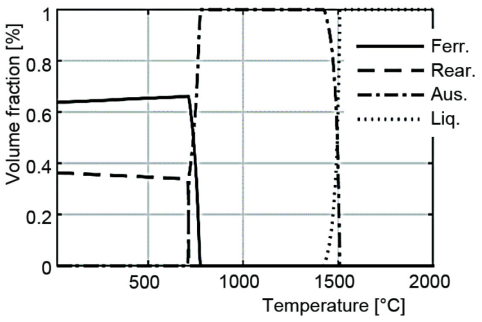

Figure 3. Volume fractions of phase constituents

Density

Density of phase mixture can be calculated [24]:

$$\rho = \frac{1}{\dfrac{f_\alpha}{\rho_\alpha} + \dfrac{f_{\mathrm{cem.}}}{\rho_{\mathrm{cem.}}} + \dfrac{f_\gamma}{\rho_\gamma} + \dfrac{f_{\mathrm{liq}}}{\rho_{\mathrm{liq}}}} \tag{22}$$

Calculation of ferrite, cementite, austenite, and liquid phase density was made based on [28] using eqs. (22)-(26). Figure 4 shows results of calculation for steel P355GH.

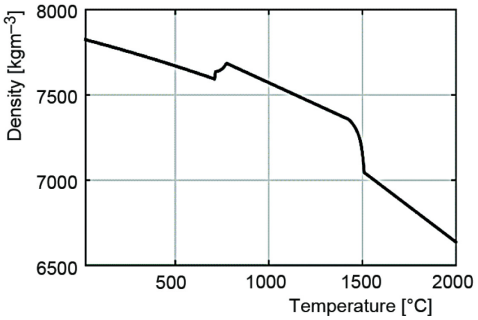

Figure 4. Density of P355GH steel *vs.* temperature

$$\rho_\alpha = (7875.96 - 0.297T - 5.62\cdot10^{-5}T^2)\cdot(1 - 0.0246C) + A_s \tag{23}$$

$$\rho_{\mathrm{cem.}} = 7686.45 - 0.0663T - 3.12\cdot10^{-4}T^2 \tag{24}$$

$$\rho_\gamma = (8099.79 - 0.506T)(1 - 0.0146\,\mathrm{C}) - 63.1\,\mathrm{Si} - 6.1\,\mathrm{Mn} - 9.3\,\mathrm{Cr} + 2.6\,\mathrm{Mo} - 0.3\,\mathrm{Ni} \tag{25}$$

$$\rho_{\mathrm{liq}} = (8319.49 - 0.835T)(1 - 0.01\,\mathrm{C}) - 67.5\,\mathrm{Si} - 3.9\,\mathrm{Mn} - 8.6\,\mathrm{Cr} + 24\,\mathrm{Mo} + 3.3\,\mathrm{Ni} \tag{26}$$

Thermal conductivity

Thermal conductivity of phase mixture can be calculated by equation:

$$\lambda = f_\alpha \lambda_\alpha + f_\mathrm{p} \lambda_\mathrm{p} + f_\gamma \lambda_\gamma + f_\mathrm{liq} \lambda_\mathrm{liq} \tag{27}$$

Thermal conductivity of ferrite, pearlite, and austenite was calculated based on [29] using eqs. (28) and (29):

$$\lambda_{\alpha,\mathrm{p}} = 44.01 - 3.863 \cdot 10^{-5} T^2 - 3.001 \cdot 10^{-7} T^{2.5} \tag{28}$$

$$\lambda_\gamma = 10.41 + 2.51 \cdot 10^{-8} T^{2.5} + 4.653 \cdot 10^{-1} \sqrt{T} \tag{29}$$

while density of liquid phase is assumed to have constant value, $\lambda_\mathrm{liq} = 35$ W/mK. Calculation results for steel P355GH are shown in fig. 5.

Effective heat capacity

Considering rule for phase mixtures, we can calculate effective heat capacity for P355GH steel, fig. 6 using equations [29, 30]:

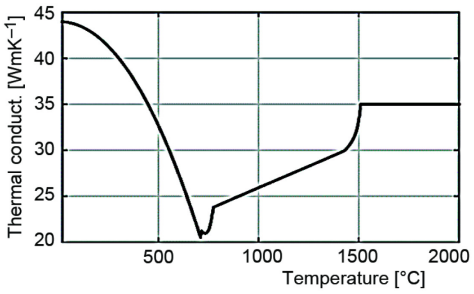

Figure 5. Thermal conductivity of P355GH steel *vs.* temperature

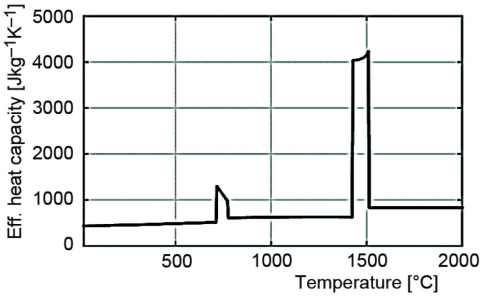

Figure 6. Effective heat capacity of P355GH steel *vs.* temperature

$$c_\mathrm{eff} = f_\alpha c_{\mathrm{p}\alpha} + f_\mathrm{p} c_{p\mathrm{p}} + f_\gamma c_{p\gamma} + f_\mathrm{liq} c_{p\mathrm{liq}} + L_{\gamma\to\alpha} \frac{\mathrm{d}f_{\gamma\alpha}}{\mathrm{d}T} + L_{\gamma\to\mathrm{p}} \frac{\mathrm{d}f_{\gamma\mathrm{p}}}{\mathrm{d}T} + L_{\mathrm{liq}\to\mathrm{sol}} \frac{\mathrm{d}f_\mathrm{ls}}{\mathrm{d}T} \tag{30}$$

$$c_{p\alpha,\mathrm{p}} = 3.42 \cdot 10^6 + 1.347 \cdot 10^{-1} T^2 + 2.015 \cdot 10^4 \sqrt{T} \tag{31}$$

$$c_{p\gamma} = -4 \cdot 10^{-8} T^3 + 4 \cdot 10^{-5} T^2 + 9 \cdot 10^{-2} T + 532 \tag{32}$$

Specific heat capacity of liquid phase is set to $c_{p\mathrm{liq}} = 830$ Jkg^{-1}K^{-1}. Latent heat of austenite to ferrite and austenite to pearlite transformation can be calculated:

$$L_{\gamma\to\alpha} = 1.25 \cdot 10^8 + 3.34 \cdot 10^6 T - 4.33 \cdot 10^3 T^2 \tag{33}$$

$$L_{\gamma\to\mathrm{p}} = 7.14 \cdot 10^8 + 2.09 \cdot 10^6 T - 3.18 \cdot 10^3 T^2 \tag{34}$$

Latent heat of melting is set to $L_{\mathrm{sol}\to\mathrm{liq}} = 280000$ J/kg.

Experiment

Experiment was carried out on P355GH steel plate with dimensions 298 × 150 × × 5 mm, fig. 7. Filler material used was OK Autrod 12.50 wire, with 1.0 mm diameter. As a shielding gas, we have used Arcal 5 (82%Ar + 18%CO_2). Temperature acquisition was made using AHLBORN Almemo 5690-2 system, fig. 8.

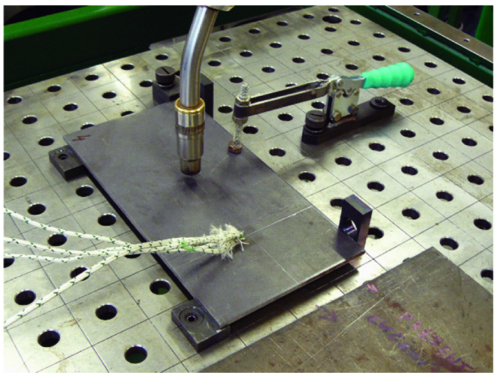

Figure 7. Experimental set-up

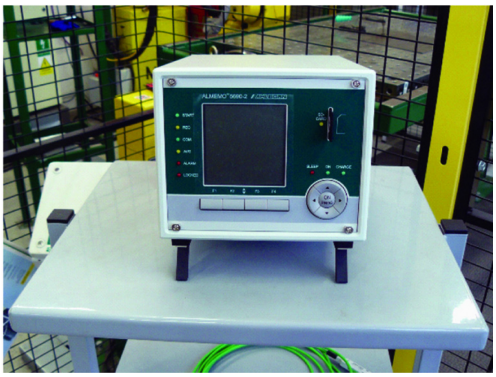

Figure 8. Data acquisition system

Temperatures were measured at four points on the upper side of welded plates, fig 9. Table 2 shows exact position of thermocouples in x-y co-ordinate system.

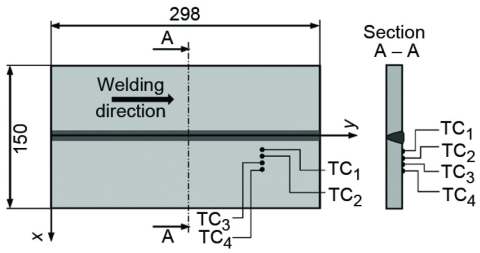

Figure 9. Position of thermocouples on the steel plate

Table 2. Co-ordinates of measurement points

	x [mm]	*y* [mm]
TC_1	10	228
TC_2	15	228
TC_3	20	228
TC_4	25	228

The experiment was conducted with following welding parameters: welding current I = 150 A, arc voltage U = 18.2 V, welding speed v_w = 0.004 m/s, wire speed v = 5.9 m per miunte, gas flow q = 8 l per minute, temperature of plate T_p = 21.6 °C, and atmosphere temperature, T_a = 20.6 °C.

Optimization method

Simulated annealing is global optimization technique based on random search. Idea for simulated annealing comes from recrystallization process throughout metal annealing. Detailed explanation of simulated annealing optimization method can be found in [31, 32].

Objective function, eq. (35), is defined as sum of squared errors between experimental and simulated values of temperatures in grid points along x-axis. As the independent unknown parameters, we have chosen set of following six parameters: arc efficiency, three semi-axes of double ellipse heat source, emissivity and effective thermal conductivity, eq. (35). The optimization procedure intends to minimize objective function in order to obtain values of unknown parameters.

$$O(x) = \sum_{i=1}^{4}\sum_{j=1}^{m}\left(\frac{T_{ij}^{\exp} - T_{ij}^{\sin}}{T_{ij}^{\exp}}\right)^2, \qquad x = \left\{\eta, \frac{a_{\mathrm{hf}}}{a_{\mathrm{hf}}^m}, \frac{a_{\mathrm{hb}}}{a_{\mathrm{hb}}^m}, \frac{b_{\mathrm{h}}}{b_{\mathrm{h}}^m}, \varepsilon, \frac{\lambda}{\lambda^m}\right\} \tag{35}$$

where

$$a_{\mathrm{hf}}^m = 0.0024 \text{ m}, \quad a_{\mathrm{hb}}^m = 0.0096 \text{ m}, \quad b_{\mathrm{h}}^m = 0.0074 \text{ m}, \quad \lambda^m = 35 \text{ Wm}^{-1}\text{K}^{-1} \tag{36}$$

Numerical simulation and optimization procedure were performed using MATLAB software package. Simulated annealing algorithms have been implemented with fast annealing function and exponential temperature update function. Initial temperature was set to 50 while reannealing interval was set to 100. Evolution of objective function value is shown on figs. 10 and 11.

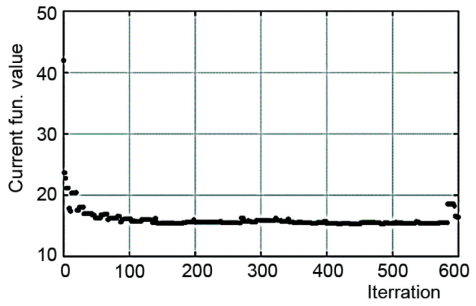

Figure 10. Evolution of current function value in function of iteration number

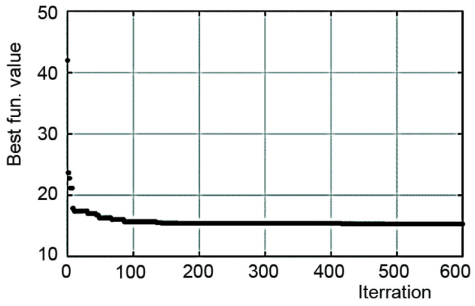

Figure 11. Evolution of best function value in function of iteration number

After optimization, we have got following values of the six unknown parameters:

$$\eta^o = 0.656, \qquad a_{\mathrm{hf}}^o = 0.00243 \text{ m}, \qquad a_{\mathrm{hb}}^o = 0.00696 \text{ m}, \qquad b_{\mathrm{h}}^o = 0.00296 \text{ m},$$
$$\varepsilon^o = 0.2003, \qquad \lambda^o = 130.24 \text{ Wm}^{-1}\text{K}^{-1}$$

Using optimized values of arc efficiency, heat source parameters, emissivity and effective conductivity, we made comparison of simulated and measured values of temperature in points shown in fig. 9 and tab. 2. Figures 12-15 show results of comparison.

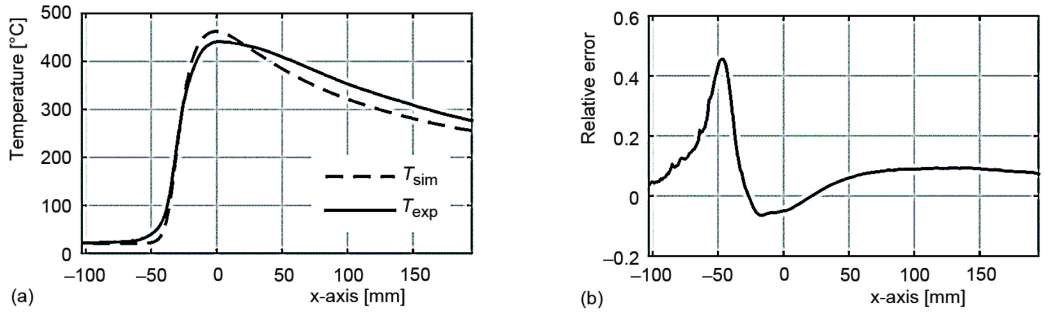

Figure 12. Comparison between simulated and measured temperatures (for TC_1) and relative error of simulation

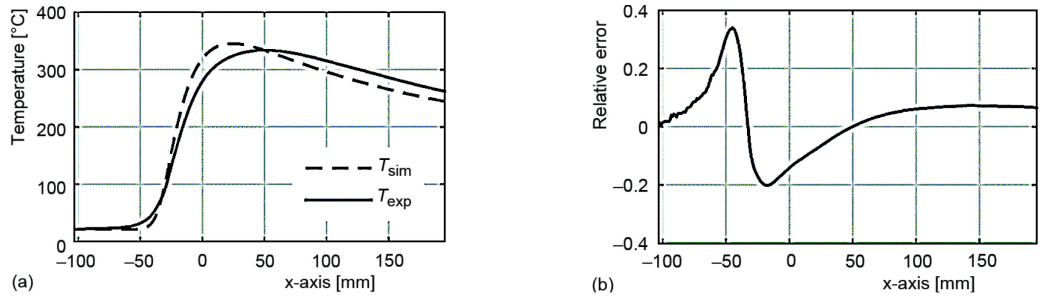

Figure 13. Comparison between simulated and measured temperatures (for TC_2) and relative error of simulation

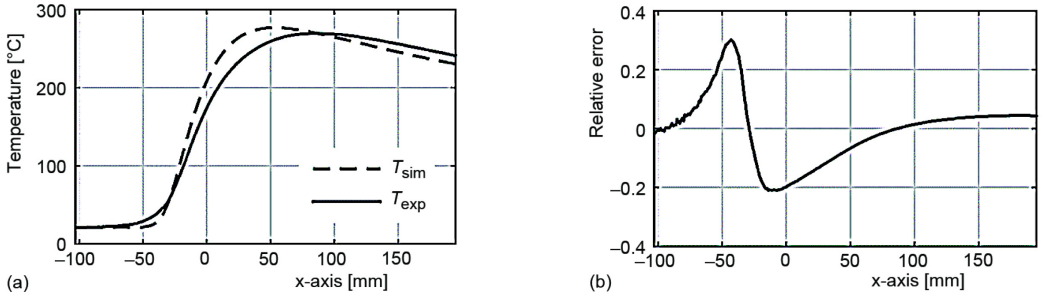

Figure 14. Comparison between simulated and measured temperatures (for TC_3) and relative error of simulation

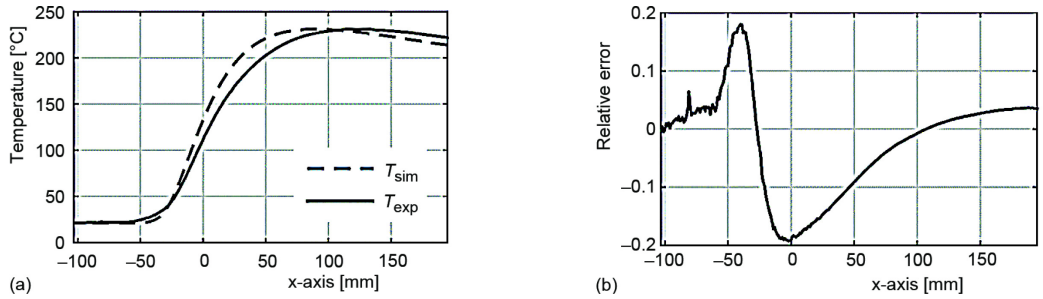

Figure 15. Comparison between simulated and measured temperatures (for TC_4) and relative error of simulation

Summary and conclusions

In order to improve accuracy of numerical model of heat transfer for GMAW, we have developed a calibration procedure for determination of six unknown parameters: arc efficiency, three semi-axes of double ellipse heat source, emissivity of steel plate surface, and effective conductivity. Procedure is based on global optimization algorithm and measurement of temperatures in four points at upper side of welded plates. Result of this procedure is a model, which gives reasonable values of temperature in comparison with experiment. Difference between measured and simulated results can be explained as a consequence of implementation of 2-D, instead of 3-D heat transfer model, considering thickness of plate. In addition, number of iterations of simulated annealing procedure was limited due to reduction of computational time, so optimized values may not be the global one. Despite all, we believe that described procedure can be successfully used for determination of uncertain parameters of heat transfer model.

Acknowledgment

The authors wish to express their gratitude to National CEEPUS Office of Czech Republic (project CIII-HR-0108-07-1314) and to the Ministry of Education and Science of the Republic of Serbia (project TR37020).

Nomenclature

Ae_1 – lower equilibrium austenite formation temperature, [°C]
Ae_3 – upper equilibrium austenite formation temperature, [°C]
A_s – correction coefficient (in this case value of A_s is set to be 0)
a_{hf} – semiaxis of front half-ellipse in x-direction, [m]
a_{hb} – semiaxis of rear half-ellipse in x-direction, [m]
b_h – semiaxis of front half-ellipse in y-direction, [m]
C – carbon content, [%]
C_{eut} – eutectoid carbon content
c_{eff} – effective spec, heat, [$Jkg^{-1}°C^{-1}$]
c_p – specific heat capacity, [$Jkg^{-1}K^{-1}$]
f – volume fraction, [%]
Gr – Grashof number
h – heat transfer coefficient, [$Wm^{-2}K^{-1}$]
I – welding current, [A]
L – latent heat, [Jkg^{-1}]
l_k – characteristic length, [m]
Pr – Prandtl number
Q – arc power, [W]
q_f – front heat source density, [Wm^{-2}]
q_l – heat source density, [Wm^{-2}]
q_b – rear heat source density, [Wm^{-2}]
T – temperature, [°C]
t – plate thickness, [m]
U – arc voltage, [V]
v – speed, [ms^{-1}]
Δx – mesh size in x-direction, [m]
Δy – mesh size in y-direction, [m]

Greek symbols

δ – overall mesh size, [m]
ε – emissivity
η – arc efficiency, [%]
λ – thermal conductivity, [$Wm^{-1}°C^{-1}$]
ρ – density, [kgm^{-3}]
σ_c – Stefan-Boltzmann constant, [$Wm^{-2}K^{-4}$]
τ – time, [s]

Subscripts

a – atmospheric
cem. – cementite
i – position of mesh node in x-direction
j – position of mesh node in y-direction
liq. – liquidus
p – pearlite
sol. – solidus
w – welding
α – ferrite
γ – austenite

Superscripts

m – measured
o – optimal

References

[1] Rosenthal, D., The Theory of Moving Sources of Heat and its Application to Metal Treatments. *Transactions ASME*, *43* (1946), 11, pp. 849-866
[2] Rykalin, N. N., Calculations of Thermal Processes in Welding (in Russian), Mashgiz, Moscow, 1951
[3] Wu, C. S., *Welding Thermal Processes and Weld Pool Behaviors*, Taylor & Francis, Boca Raton, Fla., USA, 2011
[4] Myers, P. S., *et al.,* Fundamentals of Heat Flow in Welding, *Welding Research Council Bulletin*, (1967), 123, pp. 1-47
[5] Pavelić, V., *et al.,* Experimental and Computed Temperature Histories in Gas Tungsten-Arc Welding of Thin Plates, *WELD J*, *48* (1969), 7, pp. 295s-305s.
[6] Hibbitt, H. D., Marcal, P. V., A Numerical, Thermo-Mechanical Model for the Welding and Subsequent Loading of a Fabricated Structure, *Computers & Structures*, *3* (1973), 5, pp. 1145-1174
[7] Krutz, G. W., Segerlind, L. J., Finite Element Analysis of Welded Structures, *Welding Journal Research Supplement*, *57* (1978), July, pp. 211s–216s.
[8] Kim, C. H., *et al.,* Modeling of Temperature Field and Solidified Surface Profile During Gas–Metal Arc Fillet Welding, *Journal of Applied Physics*, *94* (2003), 4, pp. 2667-2679

[9] Kumar, A., DebRoy, T., Heat Transfer and Fluid Flow During Gas-Metal – Arc Fillet Welding for Various Joint Configurations and Welding Positions, *Metallurgical and Materials Transactions A*, *38* (2007), 3, pp. 506-519
[10] Traidia, A., Roger, F., Numerical and Experimental Study of Arc and Weld Pool Behaviour for Pulsed Current GTA Welding, *International Journal of Heat and Mass Transfer*, *54* (2011), 9-10, pp. 2163-2179
[11] Pardo, E., Weckman, D. C., Prediction of Weld Pool and Reinforcement Dimensions of GMA Welds Using a Finite-Element Model, *Metallurgical Transactions B*, *20* (1989), 6, pp. 937-947
[12] Quinn, T. P., *et al.,* Coupled Arc and Droplet Model of GMAW, *Science and Technology of Welding & Joining*, *10* (2005), 1, pp. 113-119
[13] Hu, J., Tsai, H. L., Modelling of Transport Phenomena in 3D GMAW of Thick Metals with V Groove, *Journal of Physics D: Applied Physics*, *41* (2008), 6, p. 065202
[14] Xu, G., *et al.,* Three-Dimensional Modeling of Arc Plasma and Metal Transfer in Gas Metal Arc Welding, *International Journal of Heat and Mass Transfer*, *52* (2009), 7-8, pp. 1709-1724
[15] Schnick, M., *et al.,* Modelling of Gas–Metal Arc Welding Taking into Account Metal Vapour, *Journal of Physics D: Applied Physics*, *43* (2010), 43, p. 434008
[16] Mishra, S., Tailoring Weld Geometry and Composition in Fusion Welding Through Convective Mass Transfer Calculations, Ph. D. thesis, The Pennsylvania State University, Philadelphia, Penn., USA, 2006
[17] Pittner, A. A., Contribution to the Solution of the Inverse Heat Conduction Problem in Welding Simulation, Ph. D. thesis, Technischen Universität Berlin, Berlin, 2012
[18] Kumar, A., DebRoy, T., Guaranteed Fillet Weld Geometry from Heat Transfer Model and Multivariable Optimization, *International Journal of Heat and Mass Transfer*, *47* (2004), 26, pp. 5793-5806
[19] Kumar, A., DebRoy, T., Tailoring Fillet Weld Geometry Using a Genetic Algorithm and a Neural Network Trained with Convective Heat Flow Calculations, *Welding Journal*, *86* (2007), 1, pp. 26s–33s
[20] Kumar, A., DebRoy, T., Improving Reliability of Modelling Heat and Fluid Flow in Complex Gas Metal Arc Fillet Welds – Part II: Application to Welding of Steel, *Journal of Physics D: Applied Physics*, *38* (2005), 1, pp. 127-134
[21] Pittner, A., *et al.,* Fast Temperature Field Generation for Welding Simulation and Reduction of Experimental Effort, *Welding in the World*, *55* (2013), 9-10, pp. 83-90
[22] Bjelić, M., Simulation of Temperature Field During GMA Welding of Thin Sheets, M. Sc. thesis, University of Kragujevac, Kraljevo, Serbia, 2009
[23] Cengel, Y. A., *Heat Transfer: A Practical Approach*, McGraw-Hill, New York, USA, 2003
[24] Miettinen, J., Louhenkilpi, S., Calculation of Thermophysical Properties of Carbon and Low Alloyed Steels for Modeling of Solidification Processes, *Metallurgical and Materials Transactions B*, *25* (1994), 6, pp. 909-916
[25] Andrews, K. W., Empirical Formulae for the Calculation of Some Transformation Temperatures, *J. Iron Steel Inst*, *203* (1965), 7, pp. 721-727
[26] Guthmann, K., Convenient Casting Temperature Compared to the Solidification Point of Iron and Steel Melts (in German), *Stahl und Eisen*, *71* (1951), pp. 399-402
[27] Takeuchi, E., Brimacombe, J. K., Effect of Oscillation-Mark Formation on the Surface Quality of Continuously Cast Steel Slabs, *Metallurgical Transactions B*, *16* (1985), 3, pp. 605-625
[28] Jablonka, A., *et al.,* Thermomechanical Properties of Iron and Iron-Carbon Alloys: Density and Thermal Contraction, *Steel Research*, *62* (1991), 1, pp. 24-33
[29] De Oliveira, W. P., *et al.,* Thermomechanical Analysis of Steel Cylinders Quenching Using a Constitutive Model with Diffusional and Non-Diffusional Phase Transformations, *Mechanics of Materials*, *42* (2010), 1, pp. 31-43
[30] Ariza, E. A., *et al.,* Numerical Simulation with Thorough Experimental Validation to Predict the Build-Up of Residual Stresses During Quenching of Carbon and Low-Alloy Steels, *ISIJ International*, *54* (2014), 6, pp. 1396-1405
[31] Rao, S. S., *Engineering Optimization: Theory and Practice*, John Wiley & Sons, New Jersey, N. Y., USA, 1996
[32] Yang, X.-S., *Engineering Optimization: An Introduction with Metaheuristic Applications*, John Wiley & Sons, New Jersey, N. Y., USA, 2010

Paper submitted: April 15, 2015
Paper revised: August 10, 2015
Paper accepted: August 10, 2015